3D Biomimetic Tumor Microenvironment of HCC to Visualize the Intercellular Crosstalk between Hepatocytes, Hepatic stellate cells, and cancer cells

Chun Liu (liuch393@mail.sysu.edu.cn)
The First Affiliated Hospital of Sun Yat-sen University https://orcid.org/0000-0002-7975-9583
Yaolin Liu
Precision Medicine Institute, The First Affiliated Hospital of Sun Yat-sen University
Xiaoqian Yang
Precision Medicine Institute, The First Affiliated Hospital of Sun Yat-sen University
Dong Jiang
Orthopedic Research Institute/Department of Spine Surgery, The First Affiliated Hospital of Sun Yat-sen University
Rongcheng Hu
Orthopedic Research Institute/Department of Spine Surgery, The First Affiliated Hospital of Sun Yat-sen University
Fangli Huang
Orthopedic Research Institute/Department of Spine Surgery, The First Affiliated Hospital of Sun Yat-sen University
Zhenwei Peng
Department of Radiation Oncology, The First Affiliated Hospital of Sun Yat-sen University

Article

Keywords: 3D HCC model, tumor microenvironment, cellular spheroids, hepatic stellate cell, hepatic fibrosis.

Posted Date: July 11th, 2022

DOI: https://doi.org/10.21203/rs.3.rs-1777732/v1

Abstract

While a significant number of studies have focused on elucidating the functioning mechanisms of the Hepatocellular carcinoma (HCC) microenvironment, the intercellular crosstalk between multiple cells in the tumor microenvironment remains unclear. Here we co-cultured spheroids of HCC cells, hepatic stellate cells (HSCs), and hepatocytes in a biomimetic composite hydrogel to construct a 3D model of the HCC microenvironment in vitro. The model reproduced the major cellular components of early HCC in a biomimetic 3D microenvironment, realizing the visualization of the cellular interplay between cells and the microenvironment. Using this model, we showed the HSCs were activated when co-cultured with HCC cells and deposed collagen to remodel the microenvironment, which in turn triggered higher EMT levels in HCC cells. The hepatocytes also responded to the existence of HCC cells and the activation of HSCs in co-culture, showing the downregulated expression level of ALB, AFP, and HNF4A. This model recapitulated the activation of HSCs in the HCC microenvironment and enabled visualization of multi-cellular interplay in 3D, providing a biomimetic platform to investigate mechanisms of HCC and related hepatic fibrosis.

1. Introduction

Hepatocellular carcinoma (HCC) is the most common type of primary liver cancer in the world. While hepatic fibrosis and terminal stage cirrhosis have been well-considered as the main risk factors of HCC,[1, 2] the molecular pathogenesis of HCC has not yet been fully elucidated. In recent years, HCC development has been known to be strictly dependent on environmental cues. Accumulating studies have shown that HCC cells can manipulate stromal cells involved in fibrosis to promote the expansion of malignancy in healthy liver, where cancer cells interact with its microenvironment by activating hepatic stellate cells (HSCs), followed by the activated HSCs transformation into myofibroblast-like cells to promote fibrosis, cirrhosis and the progression of HCC in turn. While the above vicious spiral received general acceptance, the direct evidence showing how the multi-step interactions between HCC and tumor microenvironment (TME) occur is lacking. There are still missing several key pieces of information related to multi-cellular interplay in the TME to unlock the involved molecular mechanisms. The TME is a complex and dynamic cellular environment, including various cellular and non-cellular components. The major cellular components of the hepatic TME are tumor-associated fibroblasts and HSCs, where the activation of HSCs and the subsequent cellular and intercellular events in TME lay the foundation for exploring molecular mechanisms of fibrosis and hepatocarcinogenesis.[3] Although many studies have focused on the cellular and molecular regulators involved in HSC activation and how they contribute to TME remodeling and evolution, due to the heterogeneity and complexity of the TME, the crosstalk between the cancer cell, activated HSCs, and hepatocytes in hepatic TME has not been well understood. Specifically, investigation of the dialogue between various cells and subsequent changes in TME has been limited by the currently available modeling strategies, thus necessitating an *in vitro* hepatic TME model with adequate spatial/structural resolution to reproduce and visualize intercellular crosstalk in real time.

Although the animal model remains the current standard approach for cancer research, there are still many concerns regarding the time consuming and the lack of in-depth and real-time resolution to show cellular and molecular events *in vivo* limit its application in studying cell-cell communications.[4] The conventional 2D monolayer cell culture methods cannot reflect the 3D spatial arrangement and morphology of cells *in vivo*. Hence, they can only provide a simplified and unrealistic microenvironment. HSCs are usually activated spontaneously in 2D prolonged culture on plastic dishes.[5] However, these problems can be solved in 3D cell culture. Synthetic hydrogels can provide controlled and determined environments by controlling chemical parameters and providing the bioactive features of selective materials. 3D cell culture model has been demonstrated to be an essential biomimetic research model to bridge the gap between 2D cell culture and animal model. [6] Cancer cells cultured in the 3D biomimetic hydrogel environment showed significant differences in transcriptomics from the 2D culture.[7, 8]

Various 3D models have been applied to study hepatic fibrosis and hepatic cancer increasingly. Calitz et al. designed a 3D bionic hepatic cancer model with adjustable biophysical properties, which was applied to test the drug resistance of HCC patients.[9] By using 3D suspension droplet culture technology, Prestigiacomo et al. constructed a hepatic fibrosis model including hepatocytes, Kupffer cells, and stellate cells, which reproduced cell events such as hepatocyte injury, the activation of macrophage and stellate cells, and ECM deposition.[10] Marie et al. constructed a co-cultured model with HepaRG, stellate cells, and endothelial cells through 3D bioprinting technology, which confirmed the importance of different cell interactions for collagen deposition and hepatic fibrosis.[11] In comparison, previous studies have typically concentrated on the models of hepatic fibrosis. Although the few existing 3D models enabled the study of more complicated phenomena in hepatic fibrosis, most of them failed to recapitulate the interactions between the different constituents of the hepatic TME during tumorigenesis. Although some studies tried to imitate spatial structure by using 3D bioprinting technology, gelma, the most commonly used bioinks, is not an extracellular matrix. That is why gelma is not biomimetic enough. There has not been a 3D hepatic TME model *in vitro* that can mimic both the structure and function *in vivo*, with a real-time monitor of the cell-cell interaction during the hepatocarcinogenesis.

We previously established a series of 3D tumor models using collagen/alginate hybrid hydrogel, which possesses a well-organized, homogenous microstructure with adjustable mechanical stiffness and permeability. We have shown the follow-the-leader migration in the 3D biomimetic TME model where fibroblasts lead the invasion of cancer cells similar to *in vivo*.[12] We also demonstrated that human mammary fibroblasts could remodel the collagen network to oriented, thicker fibrillar tracks in those biomimetic hydrogels, facilitating the invasion of tumor cells.[13] Furthermore, we have demonstrated the heterogeneous stiffness in TME can induce different proliferation, migration, angiogenesis, and metabolism behaviors in cancer cells.[14] Based on these results, we further constructed a 3D model of the hepatic TME using a biomimetic hydrogel composed of hyaluronic acid (HA), type I collagen, and sodium alginate, which possesses similar components to the extracellular matrix (ECM) in HCC microenvironment. The stiffness of our biomimetic hydrogel is 182.96 ± 62.55 Pa which has been adjusted to match the stiffness of culturing HSC. [9, 15, 16]

We co-cultured spheroids of human-derived HCC cells, HSCs, and normal hepatocytes in the biomimetic hydrogel to mimic the early HCC progression into the normal liver. The spheroids embedded in gels can better reproduce the 3D microstructure of the hepatic tissue and also realize the visualization of the interaction mechanism between cells and the microenvironment. Using this model, we recapitulated the crosstalk between HCC and cellular components in TME and monitored the subsequent effects on normal hepatocytes in the surrounding. Our TME model gives a better reflection of the real HCC setting and thus can provide a versatile platform for in-depth study of cell-cell interaction, tumor development, and metastasis mechanism in the early HCC. The model we presented here can also be applied for the selection of new clinical targets for the diagnosis and therapeutics of HCC.

2. Methods

Cell culture

HL-7702 cells, LX2 cells, and MHCC-97H cells were purchased from iCell Bioscience Inc (Shanghai) cell bank. HL-7702 and LX2 were cultured in 1640 (GIBCO) and MHCC-97H was cultured in DMEM (GIBCO). These media were supplemented with 10% fetal bovine serum (GIBCO) and 1% penicillin-Streptomycin (GIBCO) in a humidified 37°C tissue culture incubator with 5% CO_2. According to -the manufacturer's instructions, the lentiviral solutions (pSLenti-EF1a-EBFP2-P2A-Puro-CMV-MCS-3Flag Lentivirus; pLenti-CBh-3FLAG-luc2-tCMV-tdTomato-F2A-Puro Lentivirus; pSLenti-CMV-EGFP-3FLAG-PGK-puro Lentivirus) purchased from OBiO Technology (Shanghai) Co.; Ltd. was used for cell infection. Specifically, the target cells in good condition were seeded into the 24-well plate, and the plate was made with a density of 5–10 ×10^4 cells/ well. After changing the culture medium on the second day, the corresponding amount of virus was added according to the formula (cell number ×MOI value/viral primordial titer) ×10^3. Cell status was observed after 8–12 hours of virus infection, and fluorescence expression was observed on the fifth day. After screening, a stable transformation of HL-7702-GFP, MHCC-97H-BFP, and LX2-Tomatoes was obtained, and expanded culture was conducted.

Preparation of cell spheroids

We prepared spheroids with HL-7702, MHCC-97H, and LX2 as described above. Briefly, we added 2.5×10^5 cells in 20 μl culture medium to 384-well low volume, non-adhesive, round-bottom plates (Corning) and cultured cells for 48 hours before embedding them in gels.

Hydrogel preparation

We prepared hydrogels by modifying the previous protocol with the addition of HA.[13] The pre-gel contains 3 mg/ml collagen (Ibidi), 5 mg/ml alginate (Sigma Aldrich), and 1mg/ml HA (Sigma Aldrich) as major components, with 7.5 mM CaCl2 (Sigma Aldrich) as a crosslinker.

Establishment of the 3D HCC microenvironment

The spheroids with HL-7702, LX2, and MHCC-97H were encapsulated in hydrogel for 3D culturing. The ratio of HL-7702, LX2, and MHCC-97H was 5:2:1. This means that there were 20 HL-7702 cell spheroids, 8 LX2 cell spheroids, and 4 MHCC-97H cell spheroids in the three co-cultures (3CO). Similarly, in two co-cultures (2CO) of HL-7702 with LX2, there were 20 HL-7702 cell spheroids and 8 LX2 cell spheroids. For cultured alone, there are 20 HL-7702, 8 LX2, and 4 MHCC-97H, respectively. Tumor spheroids were mixed with the pre-gel and cultured in a 15mm glass-bottom cell culture dish (801002, Nest Biotechnology). The pre-gel was cured at 37°C in the incubator, and a fresh cell culture medium was added after 30 mins. Mixed cell spheroids were cultured in 1640/DMEM (the mixed ratio was 7/1) complete culture medium. The culture medium was changed every 2 days.

Fluorescence microscope

We captured all microscopic images of cells and spheroids with an inverted fluorescence microscope (OLYMPUS IX83) and a two-photon microscope (Leica TCS SP8 DIVE) with HC FLUOTAR L 25x/0.95 WATER. We used 840 nm excitation for GFP, 1020 nm excitation for red fluorescent proteins, 760nm excitation for blue fluorescent proteins, and 930nm excitation for collagen (second harmonic generation), collecting emitted light in green (495–505 nm), red (560–570 nm), blue (406–485 nm) and collagen (460-470nm) channels, respectively. We stitched images with a resolution of 1024×1024 to show the entire field. We used the same acquisition parameters for all cells and spheroids compared within a single experiment. We exported images to Imaris (Imaris V9.0, Bitplane Inc) for image segmentation and data analysis.

Nanoindentation

Young's moduli of hydrogels were measured with a Piuma Nanoindenter (Optics 11) using a cantilever with a spring constant of 0.260 N/m and a tip radius of 25.500 μm. The measurements were conducted in PBS. The area of Young's modulus maps was 2000 × 2000 μm^2 with an increment of 200 μm by X and Y axes. The Young's modulus for each point was computed according to the Hertzian contact mechanics model for a spherical body indenting a flat surface, using the DataViewer V2 (DataViewer V2.4.0, Optics 11). Based on the measurement results, the effective Young's modulus (E) of a sample was calculated as mean ± standard deviation (SD).

Quantification of collagen deposition

As described above, we took fluorescent images on day 2, 5, and 7 and analyzed images using Imaris software. For intensity determination, we used the surface module to compute the intensity of the final day's image. The sum of intensity in each sample was analyzed in GraphPad Prism 9.2.0 (GraphPad Software, La Jolla, CA) to show the difference in collagen deposition between the HCC microenvironment model, co-culture system of HL-7702 spheroids, and LX2 cell spheroids, and LX2 cell spheroids single-cultured system. All data were expressed as mean ± standard deviation (SD).

Quantification of HL-7702 proliferation

Likewise, as described above, we took fluorescent images on day 0, 1, 2, 5, and 7 and analyzed images using Imaris software. The total area of each HL-7702 sample was measured using the Imaris surface function. The area of day 0 was set up as 100%. Statistical analyses were performed using Prism software to show the changes and the trend of the HL-7702 area between the HCC microenvironment model, co-culture system of HL-7702 spheroids, and LX2 cell spheroids, and HL-7702 cell spheroids single-cultured system. All data were expressed as mean ± standard deviation (SD).

Quantification of MHCC-97H cell migration

At large scales, fluorescent images were acquired using an inverted fluorescent microscope as described on day 0, 1, 2, 5, and 7 and analyzed using Imaris software. Similarly, we created the surface to render the area of MHCC-97H and computed the total area of each sample. The area of day 0 was set up as 100%. Statistical analyses were performed using Prism software to show the changes and the trend of the MHCC-97H area between the HCC microenvironment model and the MHCC-97H cell spheroids single-cultured system. All data were expressed as mean ± standard deviation (SD).

On the cellular scale, we also took the fluorescent images by two-photon microscope as described and analyzed them using Imaris software. For visual normalization, images were analyzed using the spot model analysis tool to mark every single cell. We set the center of the cell spheroids as the coordinate origin. All spots were represented in a color spectrum with a range of 10–90 μm (on day 2) and 10–360 μm (on day 5). Statistical analysis was conducted using the Kolmogorov-Smirnov test between MHCC-97H cultured alone and the HCC microenvironment model by Prism software. A value of $p \leq 0.05$ was used as a threshold for statistical significance. All data were expressed as mean ± standard deviation (SD).

RNA extraction and RT-qPCR assay

After 3 or 7 days of culture, we washed gels from different conditions using PBS three times and then incubated the gels with 50 mg/ml sodium citrate for 5–10 minutes, followed by 1 mg/ml collagenase lysis. Then, each cell was obtained by flow cytometric sorting (BD FACSAria SORP). The total RNA was extracted by TRIzol reagent (Invitrogen), and the concentration was measured by the quantitation analyzer for nucleic acids (Implen N60 Touch). The cDNA was synthesized using the HiScript ® RT SuperMix for qPCR (+ gDNA wiper) kit (Vazyme), and the qPCR reaction was performed using ChamQTM SYBR Green qPCR Master Mix (Low ROX Premixed) (Vazyme). The primers were purchased from Synbio Technologies Co., Ltd. The expression levels of genes were quantified using the comparative Ct method. Also, the expression level of each mRNA was normalized to the expression of GAPDH mRNA and calculated as the fold difference relative to the control.

The human primer sequences used in qPCR are shown as below:

GAPDH: GCTCACTGGCATGGCCTTCCG; GTGGGCCATGAGGTCCACCAC

ALB: TGCAACTCTTCGTGAAACCTATG; ACATCAACCTCTGGTCTCACC

AFP: CTTTGGGCTGCTCGCTATGA; GCATGTTGATTTAACAAGCTGCT

HNF4A: CACGGGCAAACACTACGGT; TTGACCTTCGAGTGCTGATCC

CYP3A4: AAGTCGCCTCGAAGATACACA; AAGGAGAGAACACTGCTCGTG

CYP3A7: AAACTTGGCCGTGGAAACCT; CCTTACGGAAGGACAAAGCATTT

TGFβ1: GGCCAGATCCTGTCCAAGC; GTGGGTTTCCACCATTAGCAC

αSMA: AAAAGACAGCTACGTGGGTGA; GCCATGTTCTATCGGGTACTTC

TIMP1: CTTCTGCAATTCCGACCTCGT; ACGCTGGTATAAGGTGGTCTG

Snail: CGAACTGGACACACATACAGTG; CTGAGGATCTCTGGTTGTGGT

Twist: GTCCGCAGTCTTACGAGGAG; GCTTGAGGGTCTGAATCTTGCT

N-cadherin: TCAGGCGTCTGTAGAGGCTT; ATGCACATCCTTCGATAAGACTG

E-cadherin: CGAGAGCTACACGTTCACGG; GGGTGTCGAGGGAAAAATAGG

Integrin α6β1: CCTACTTCTGCACGATGTGATG; CCTTTGCTACGGTTGGTTACATT

ICAM-1: ATGCCCAGACATCTGTGTCC; GGGGTCTCTATGCCCAACAA

Statistical analysis

Before mapping the data on GraphPad Prism 9.2.0, we used Microsoft Excel to process qPCR data. Unless explicitly stated in the title, all variables are expressed as the average of at least three technical repeat tests ± standard deviations (SDS). T-test or one-way analysis of variance (ANOVA) was used to evaluate the difference between the average values of each group, and P-value(≤ 0.05)) was used to represent the significant difference.

3. Result

3.1. Construction of 3D biomimetic HCC microenvironment model *in vitro*

We seeded the cell spheroids stained by fluorescence in our 3D biomimetic model (Fig. 1a). Each cell spheroids were placed in a specific spatial structure to mimic the TME *in vivo*. As can be seen from Fig. 1b, the microscope can provide accurate real-time observation of the morphological changes, cell contact, proliferation, and apoptosis of cells in the microenvironment. These cells can also be extracted at any time for biological characterization.

We also used nanoindentation to determine Young's modulus of the hydrogel (Fig. 1c-d). The resulting Young's modulus map shows that the values range from 58.04 to 312.89 Pa. In the image, contrast no longer indicated height but rather Young's modulus: brighter colors indicate harder areas. According to the Hertzian contact mechanics model, Young's modulus of the hydrogel was 182.96 ± 62.55 Pa, indicating a cell culture-adapted environment.

We observed and recorded the formation of hepatic canaliculi and canaliculi-like structures (Fig. 1e) cultured in the hydrogel system, which symbolized hepatocytes differentiated into mature.[17] The lucent rim surrounding each hepatocyte represents the presence of hepatic canaliculi. During the research, we found that normal hepatocyte spheroids can be aggregated continuously and organized into a microstructure similar to lumen over time in the 3D gel culture, which accords with the research results of Landry et al., who seeded rat hepatocytes on a non-adhesive plastic substrate, then found that hepatocytes regrouped in hepatocyte islands, viz. the central lumen, within a few days.[18] Our results indicate that the microenvironment model of HCC is mature and likely to mimic the microstructure in real organs.

3.2. Activated hepatic stellate cell induced by hepatoma cells promotes hepatic fibrosis

We observed morphological changes in hepatic stellate cells in the red fluorescent area of Fig. 2a. Unlike 2D culture, HSCs showed similar trends of cell morphology changes under all three different co-culture conditions due to the cellular morphology determined by matrix composition, while collagen provides abundant cellular binding sites. Since we could not determine the activation status of HSCs by cell morphology, collagen deposition and RT-qPCR were used to determine whether HSCs were activated.

We detected the collagen network (pseudo-colored in white) with second harmonic imaging (SHG) using two-photon microscopy, observed, and conducted a continuous tracking of collagen deposition in the system. Figure 2b indicates that the changes in collagen deposition can be seen in the two-photon images. In the condition of fibrosis, HSCs secrete a large amount of extracellular matrix around hepatocytes, which affects the material exchange between cells and blood, affecting the normal function of hepatocytes and resulting in the hypoxia microenvironment around tumor cells.[19] Thus, we used fluorescence intensity to quantify the deposition of collagen to evaluate the degree of liver fibrosis. The fluorescence intensity data may not conform to a normal distribution because of its discrete nature. Therefore, we used the mean and median intensity to corroborate each other. As shown in the violin chart of Fig. 2c, we analyzed the fluorescence intensity of Day 7 by Imaris and illustrated that the collagen deposition increased from single-culture to 3CO. Further analysis also shows that the collagen deposition of 3CO exceeded that of 2CO, which means HCC cells can promote liver fibrogenesis in the HCC microenvironment. The two-photon images also evidenced this phenomenon. During the cultivation, compared LX2 cultured alone to 3CO, LX2 was spontaneously re-aggregated and formed the collagen into cluster-like structures, while 3CO was covered with visible crossed collagen bundles.

In order to further confirm whether HSCs have been activated, we continue to detect the activation-associated gene expression in HSCs (Fig. 2d). α-SMA is a known molecular marker for activated HSCs.[20] We confirmed by RT-qPCR that when LX2 is cultured alone or co-cultured with 7702, the expression of α-SMA was low or not detected. However, when HCC cells were present in the co-culture system, α-SMA was in high gene expression. The same result was obtained in TIMP1, especially on day 7. The activated HSCs secreted tissue-specific inhibitors, such as TIMP1, to sustain and increase fibrogenesis and thus positively promote the proliferation and survival microenvironment for HCCs when the transformation of normal hepatic cells has occurred.[21–23] We also detected the gene expression of TGFβ-1, which is also known as a growth factor to cause activation of quiescent HSCs and significatively induce collagen secretion.[11] The gene expression of LX2 alone, 2CO, and 3CO showed an upward gradient trend on both day 3 and day 7. These results indicate that HSCs have been activated by HCC cells in the co-culture system. Likewise, the HCC cells co-cultured in our HCC microenvironment model induced HSCs activation and may further promote the formation of hepatic fibrosis.

3.3 Effect of activated hepatic stellate cells on normal hepatocytes

As a preliminary step, we assessed the proliferative effect of 7702 by tracking their growth rate. Since we were using cell spheroids, it is difficult for live/dead staining to effectively penetrate inside the cell spheroids, so we used the sum of area of green fluorescence to confirm whether the cells were alive or not. In Fig. 3a, all images were photographed with an Olympus fluorescence microscope and were analyzed with Imaris to calculate the total area of 7702 (green fluorescent). The area of day 0 was set as 100%. The result (Fig. 3b) shows that the number of 7702 cultured alone reached a peak on day 1 and then gradually fell back. In contrast, the number of 7702 in 3CO was relatively more stable as the cells barely proliferated and showed a gentle increasing apoptosis level with culture time. The situation of 2CO was in-between.

To further investigate how TME influenced 7702, we detected alteration of gene expression in normal hepatocytes in the co-culture system to reveal the effect of activated HSCs on normal hepatocytes. In our previous study, we have experimentally confirmed that HCCs can increase the gene expression of TGFβ-1 in 3CO by activating HSCs. Furthermore, a high level of TGFβ-1 in the microenvironment can induce the decrease of ALB (albumin), AFP (alpha-fetoprotein), and HNF4A (hepatocyte nuclear factor alpha) gene expression in hepatocytes.[11, 24, 25] One of the most important functions of liver cells is ALB.[26] When the liver is damaged, ALB levels decrease.[27, 28] In addition, AFP is produced in response to the stimulus of liver diseases such as hepatitis, cirrhosis, liver cancers, and cholangiocarcinoma.[29, 30] Besides, HNF4A is overexpressed in hepatocytes.[31] It is also necessary for cell differentiation by ensuring the expression of intermediary genes required for the metabolism of glucose and lipids.[32] HNF4A has been described as conferring chemoresistance in tumors, where it has been the most upregulated gene after hypoxic conditions. It was reported that high expression levels of HNF4A have been correlated with poor prognosis.[33] As shown in Fig. 3c, ALB, AFP, and HNF4A specifically expressed in hepatocytes were upregulated when single cultured to 2CO but down-regulated when cultured from 2CO to 3CO. Also, the

expression of AFP and HNF4a showed no significant difference on day 3 and day 7. These results represented that HCCs can inhibit normal hepatocytes growth during the whole time being cultured in 3CO.

In addition, we detected the gene expression of CYP3A4 and CYP3A7. According to previous studies, cytochrome P450 (CYP) 3A enzymes are the most important human drug-metabolizing enzymes. In adults, CYP3A4 is the primary CYP3A enzyme, whereas CYP3A7 is the primary enzyme in fetuses. [34–37] The results illustrated that the expression of CYP3A4 and CYP3A7 genes increased from single culture to 2CO but decreased from 2CO to 3CO on day 2. Moreover, the expression of CYP3A4 in the 3CO group increased significantly with the increase of culture time, which indicated that the metabolic activity of hepatocytes was close to that *in vivo*.[11]

3.4 The influence of hepatic fibrosis on cancer cells

We further observed and tracked the proliferation and migration of cancer cells in the HCC microenvironment model by fluorescence microscope (Fig. 4a) and analyzed the images with Imaris to calculate the total area of HCCs (blue fluorescent) (Fig. 4b). The area of day 0 was set as 100%. Noticeably, cancer cells in the co-culture system did not migrate and spread significantly. However, the proliferation of cancer cells from the center of cell spheroids to the peripheral microenvironment was more obvious in the single culture. The reason could be due to fibrosis caused by activated HSCs.

In order to elaborate on this conclusion, we scanned the spatial configuration of HCCs spheroids with a two-photon microscope (Fig. 4c). Imaging data were imported into Imaris. By using the spot mode, each fluorescent intensity of a single nucleus was assigned one spot, and thus each cell's position was extracted at the exact coordinates (x, y, z). We set the center of cell spheroids as the origin (0, 0, 0) and calculated each cell's distance to the origin. We use different colors to label each cell based on its distance from the origin. The results can be seen visually in Figure 4d.

Further, we can see from the bar chart that the average distance of migration of HCCs cultured alone was less than that of 3CO on day 2, but exceeded 3CO on day 5. The same trend was maintained on the violin chart. These are the combined results of cell proliferation and migration. The outermost edge of the cell spheroids is the invasion front, which means the migration of cell spheroids and the proliferation was indicated by the cells located closer to the center of cell spheroids. By analyzing the cell area distribution on day 2 and day 7, we can find that HCCs in single-cell culture were dispersed by spherical differentiation. Thus, the cells cultured alone concentrated in the cell spheroids' center and surface, while the HCCs in 3CO were concentrated in the center of the cell spheroids. These results confirmed that the proliferation and migration ability of the tumor cells in 3CO were weaker than that in cultured alone.

We also examined the expression levels of genes related to cancer-promoting factors in liver cancer. The epithelial-mesenchymal transition (EMT) is implicated in the progression of early-stage tumors into invasive cancers. Snail is an essential set of regulators for fibrosis in various organs such as the kidney, liver, and lung.[38] Researchers found that treatment with Snails caused extracellular matrix deposition

and increased liver injury following CCl4-induced liver fibrosis in rats.[39] Invading cells remodel stromal tissue during tumor progression and invasion. It appears that Twist is a key factor in these processes. It has recently been shown that Twist expression activates dormant developmental pathways,[40] which has recently been associated with metastasis in liver cancer.[38] Importantly, a "cadherin switch "with increased N-cadherin and reduced E-cadherin expression had an independent prognostic effect on time to both biochemical failure and clinical recurrence in multivariate survival analyses, stronger than for E-cadherin or N-cadherin separately.[41] An increase in N-cadherin expression contributes to the development of a stroma-oriented cellular adhesion profile, which may indicate EMT.[40, 42, 43] Additionally, EMT is characterized by loss of expression of E-cadherin. Cell-cell adhesion junctions containing E-cadherin are required for the development of embryonic epithelia and for epithelial homeostasis in adult epithelia. There is a consistent loss of E-cadherin at sites of EMT during development and cancer. Animal models show that this loss increases tumor cell invasiveness in vitro and contributes to the transition from adenoma to carcinoma.[40, 44] As shown in Fig. 4e the gene expression of Snail, Twist and N-cadherin in HCCs was significantly increased in co-culture compared with monoculture, whereas the expression of E-cadherin decreased significantly, indicating that EMT may have occurred in the co-culture microenvironment.

The increased expression of integrin α6β1 and intercellular adhesion molecule ICAM-1 can enhance the invasion and movement ability of HCC cells and thus accelerate the progression of Hepatocellular Carcinoma.[45] Cancer cells that express integrin α6β1 have a greater propensity to invade. α6β1 may possess a pro-metastatic function in other cancers as well. The expression of α6β1 is also crucial for the attachment of hepatocellular carcinoma cells to laminin in hepatocellular carcinoma. In hepatocarcinomas, the integrin is overexpressed, suggesting that it may be involved in invasion and metastasis. Human hepatocarcinoma cells with reduced expression of α6β1 had decreased motility and invasiveness, which is consistent with this hypothesis.[46] Likewise, ICAM-1 is a cell adhesion molecule similar to immunoglobulin, which is expressed at low levels by endothelial cells (ECs) under normal circumstances. Inflammatory cells adhere to vascular endothelial cells and move across the endothelial barrier, and ICAM-1 is critical for adhesion to vascular ECs during the extravasation of inflammatory cells across the endothelial barrier.[47] ICAM-1 is barely detectable along the sinusoids and portal venules in a normal liver.[48] Cancer growth is fueled by cell adhesion molecules, such as ICAM, which allows cancer cells to migrate to distant organs and adhere to endothelial cells.[49] As described in the results, the expressions of Integrin α6β1 and ICAM-1 were significantly increased in co-culture in HCCs compared with that in the single culture. Therefore, these results suggest that HCC cells in the co-culture system should have a stronger invasion and movement ability than those cultured alone, contrary to what is observed in our model. Based on previous results, we speculated that hepatic fibrosis restricted the growth and metastasis of HCCs.

4. Discussion

The main objective of this study is to construct an *in vitro* model of the HCC microenvironment for real-time observation and precise regulation to study the interactions between tumor cells in the tumor

microenvironment. In particular, the study focuses on whether the activation of HSCs by cancer cells in the microenvironment can further cause damage to normal hepatocytes or even induce the formation of normal hepatic tissue fibrosis. Furthermore, the matrix components in the microenvironment have a significant impact on cell morphology. In order to simulate the real HCC microenvironment *in vitro*, the matrix materials should be bionic.

We optimized the material system for the model construction to restore the real situation *in vivo* to the greatest extent in material composition and properties. Previous attempts have been made to use stellate cells in culture, but *in vitro* studies of fibrosis were not considered because stellate cells often undergo spontaneous activation when grown on plastic dishes.[50] Specifically, compared to normal liver tissue (5 KPa), cell culture dishes exhibit a tissue tension that is greater than that of fibrotic/cirrhotic liver tissue (20 KPa). [5] The hTERT-HSC was shown to return to a quiescent state after cultivation on extracellular matrix components.[51] In prior research, hepatocytes have been cultured on various conditions or platforms with different mechanical properties in order to preserve a functional phenotype similar to that observed in the liver.[15, 16, 52–54] The most common way to maintain primary hepatocytes in a soft environment is through fabricating hydrogels based on ECM proteins.[9, 15, 16] HA is a naturally occurring anionic polymer and an important component of the extracellular matrix, often overexpressed in tumors. When it accumulates around tumors, it contributes to enhanced invasion of cancerous cells, cancer cell malignancy, and poor outcomes for patients. [55, 56]. It mediates processes such as cell adhesion, migration, and proliferation by interacting with cell surface receptors (e.g., CD44 and RHAMM). [57] By adding HA to the collagen-sodium alginate composite hydrogel material, Young's modulus value of the new composite gel material is 182.96 ± 62.55 Pa which provides an ideal microenvironment for cells. [58] Cell spheroids are ideal tools for studying the interaction between cells and are suitable for constructing the tumor microenvironment model simulating the effect of early hepatic cancer on normal tissues.[18, 59–61] We constructed a 3D HCC microenvironment model by mixing the new composite gel material with hepatocellular carcinoma cells, normal hepatocytes, and hepatic stellate cell spheroids. The model includes the 3D tumor microenvironment similar to the extracellular matrix *in vivo* and the tumor spheroid similar to the tumor formed by cancer cells. It can be cultured *in vitro* for over a week. This model can simulate the invasion and diffusion of cancer cells from tumors to the surrounding microenvironment and monitor the interaction of cancer cells, other cells, and the extracellular matrix.

In the culture of primary hepatocytes, maintenance of canaliculi or canaliculi-like structures (partial ducts) is a prominent indicator to ensure the specific desired phenotype.[62–65] As we have shown previously, these specific structures were successfully cultured in our hydrogel system. Hepatocytes are generally found aggregating in the deep cell spheroids and concentrated in the central lumen because of the actin remodeling.[66, 67] These canaliculi or canaliculi-like structures form partial intercellular ducts that resemble hepatic canaliculi in hepatocytes cultured. Besides, these discrete zones of deposited extracellular matrix materials contain laminin, fibronectin, and collagen. They deposited at a specific location between cells, forming precise structural units of apparently homologous cell types and ensuring that certain hepatic functions were maintained. Grover et al.[68, 69] showed that not only laminin and fibronectin produced by the cells were essential for their differentiation but moreover that the insoluble

proteins had to be deposited in a very specific pattern relative to the epithelial cells. Thus, the hepatic canaliculi and canaliculi-like structures are also a signal that hepatocytes differentiated into mature.[17] A higher level of homologous and heterologous cell-cell contacts rendered possible in a 3D structure may be another important factor in the maintenance of hepatocytes in aggregate culture. Moreover, it was shown in a previous study that collagen type I in soft conditions promoted the survival and aggregation of primary hepatocytes.[70] This study suggested that collagen type I, a considerable proportion of our hydrogel system, plays an important role in supporting cell viability and aggregation in hepatocytes cultured under soft conditions. These results suggest that our hydrogel system can simulate the real HCC microenvironment *in vitro* and support the growth of cells.

HCC develops based on pathophysiological processes such as repeated liver damage, inflammation, fibrosis, and cirrhosis.[3] HSCs are a significant participant in the TME. They interact with HCC cells and participate in the occurrence and development of tumors.[19, 71] In our TME, we cultured and tracked the activation and proliferation of HSCs successfully and compared morphological changes and collagen deposition of HSCs in different culture systems. Activated HSCs secreted extracellular matrix into ECM. They can promote ECM synthesis and inhibit ECM degradation by synthesizing TIMPs, which leads the ECM deposition to form hypertrophic scar and promote hepatic fibrosis. Previous studies have found that HSCs affect extracellular matrix balance and cause fibrosis by secreting collagen and matrix metalloproteinase inhibitors, which means HSCs can promote the occurrence of hepatic fibrosis by synthesizing a large number of collagen and tissue inhibitor TIMPs after activation.[11] Our results are consistent with previous observational studies.

As the main source of extracellular matrix, HSCs activation plays an essential role in the progression of fibrosis and the occurrence of HCC cells.[72] In our HCC microenvironment, HCC cells induced the up-regulation of TGF-β expression, which promoted the activation of HSCs. In addition, the expression of α-SMA was induced, which made HSCs obtain an activated phenotype characterized by cytoskeleton remodeling.[22, 23] Thus, the activated HSCs cells can affect the function of normal hepatocytes and the development of HCC cells. In this research, we observed that HCC cells could promote the transformation of inactive hepatic stellate cells into active ones in the HCC microenvironment model. In turn, activated hepatic stellate cells can affect the development of hepatic cancer cells, which is consistent with the existing findings.

We also observed the growth trend of normal hepatocytes in different culture systems. This study indicated that the proliferation of normal hepatocytes in single cultured and 2CO systems showed a trend of rising first and then falling, while that in 3CO were relatively stable. We speculated that there were two different kinds of growth inhibition that happened in our HCC microenvironment. One was from 7702 itself, and the other was from tumor growth inhibition. For 7702 alone and 2CO, due to the limited cultured space in the cultured system, the higher cell concentrations inhibited cell growth after day 1. However, for 3CO, cells were inhibited by HCC cells during the whole cultured time. Therefore, although the growth of 7702 was inhibited under different cultural conditions, it finally showed different states.

As noted in our previous study, HCC cells can activate HSCs which in turn influence the TME. The results show that the proliferation of normal hepatocytes in single cultured and 2CO systems was similar. Hence, it could conceivably be hypothesized that HSCs activated by HCC cells can affect the proliferation of normal hepatocytes. Normally, the liver is mainly composed of hepatic parenchymal cells and nonparenchymal hepatic cells. HCC usually originates from the malignant transformation of hepatic parenchymal cells. Also, virus infection and chronic inflammation can promote the transformation of hepatic cells into tumors.[73, 74] Meanwhile, various cytokines around hepatocytes, including hypoxia and extracellular matrix, may play a role in this process.[75] During the fibrogenesis, HSCs secrete a large amount of extracellular matrix to surround tumor cells and hepatocytes, which affects the material exchange between cells and the microenvironment, leading to the normal function of hepatocytes being affected and causing hypoxia microenvironment around tumor cells.[19] This phenomenon can be observed by detecting the alternat gene expression of normal hepatocytes compared to those cultured in a pathological model. Therefore, in order to confirm our conjecture, we further detected the activation-associated gene expression in hepatocytes. The liver-specific functional genes include ALB (encoding albumin), AFP (alpha-fetoprotein), CYP3A4 (cytochrome P450 3A4), CYP3A7 (cytochrome P450 3A7), HNF4A (hepatic nuclear factor 4-alpha). The expression and metabolic activity of cytochrome P450 proteins, including CYP3A4 and CYP3A7, are also important markers of hepatocyte function.[76] ALB and AFP are produced in response to the stimulus of liver diseases like liver cancer and HNF4A upregulated gene expression after hypoxic conditions. In our previous study, we have experimentally confirmed that HCCs can increase the gene expression of TGFβ-1 in TME by activating HSCs. Furthermore, a high level of TGFβ-1 in the microenvironment can induce the decrease of ALB, AFP, and HNF4A gene expression in hepatocytes.[11, 24, 25] Therefore, it is reasonable to infer that TGFβ-1 in the co-culture system induces the down-regulation of these genes and that the microenvironment changes caused by the activation of hepatic stellate cells may lead to the damage of normal hepatocytes and may promote the formation of hepatic fibrosis. In addition, we examined the expression of human drug-metabolizing enzymes. The results indicated that the metabolic activity of hepatocytes was close to that *in vivo*.[11] These results further support that our HCC microenvironment model can mimic the true *in vivo* tumor conditions.

EMT refers to the process of transformation of epithelial cells to phenotypic mesenchymal cells resulting in increased motility and invasiveness. During this process, cells lose polarity, cell-cell adhesion, epithelial markers such as E-cadherin, and acquire mesenchymal properties with high expression of mesenchymal molecular markers, including Snail and Twist.[77] Studies have shown that HSCs cells activated by hepatic cancer cells can affect the development of hepatic cancer in turn. Therefore, we continue to study the effect of HSCs on cancer cells. HSCs induced activation by HCC cells can reduce the expression of epithelial marker E-cadherin and increase the expression of interstitial marker N-cadherin, transcription factor Twist, and transcription inhibitor Snail. They can induce EMT of hepatic cancer cells and promote proliferation, invasion, and metastasis of cancer cells.[75, 78, 79] Secondly, the collagen secreted by HSCs forms highly cross-linked collagen bundles, making HCC cells gradually flexible and able to infiltrate the hepatic tumor matrix. HCC cells can invade and metastasize because of their ability to adhere, proliferate and degrade the extracellular matrix. Moreover, EMT is the key to the initiation of tumor

metastasis, which can enhance the mobility and adhesion of cells. The specific manifestation is that the stable structure of epithelial cells is disturbed, and mesenchymal cell phenotype is obtained, which forms significant invasion and migration behavior, and finally leads to the occurrence of metastatic tumors.[80] The integrin is a transmembrane glycoprotein adhesion molecule that mediates ECM and intercellular adhesion. The increased expression of integrin α6β1 and intercellular adhesion molecule ICAM-1 can enhance the invasion and movement ability of HCC cells, thus accelerating the process of hepatocellular carcinoma.[24]

A growing number of researches show that a solid extracellular matrix plays a structural supporting role in tumor growth and plays a vital role in regulating the invasion and metastasis of cancer cells as a component of the tumor microenvironment. Although there were significant changes in the expression of metastasis-related genes in cancer cells in the tumor microenvironment model, there were no obvious signs of migration. The reason may be related to the fibrosis caused by the activated HSCs. Amanda et al. think that the mechanical tension caused by hepatic fibrosis limits the spread of cancer cells.[81] Hepatocytes are the primary source of tissue regeneration. When the initial injury severely affects the proliferation of hepatocytes, it can involve the proliferation of hepatic progenitor cells and the activation of hepatic stellate cells. According to the latest research, the regenerative nodules produced by hepatic progenitor cells and fibrosis caused by myofibroblasts can limit the development of tumors in space, thus avoiding the spread of cancer cells and jointly inhibiting the formation of tumors, which enables cells to migrate up gradients of elastic modulus in a process known as durotaxis.[82, 83] This finding is consistent with our results. Consequently, it is also necessary to establish and improve a 3D culture platform that is more in line with the physiological environment to study the effects of matrix stiffness on proliferation, invasion, and metastasis of HCC cells.

5. Conclusion

In this study, we successfully constructed a 3D visualized bionic micro-environment model of HCC *in vitro* using the self-developed biomimetic composite hydrogel system and cells, viz. hepatoma cells, normal hepatocytes, and hepatic stellate cell spheroids. Compared with the previous studies of the interaction between a few key cytokines or cell behaviors in a single system, we systematically studied the complex interaction mechanism between cells in the whole tumor microenvironment in a real-time observation and precise regulation model for the first time (Fig. 5). Similar to the reported research conclusions, our research results confirm that hepatic stellate cells activated by cancer cells in the HCC microenvironment can cause liver injury and even hepatic fibrosis and affect the development of cancer cells in turn. Therefore, our research provides a reliable microenvironment biomimetic system for further studying the occurrence and development of HCC, which can study the interaction mechanism between microenvironment cells and the interaction relationship between cells and the extracellular matrix. This research has important clinical significance for improving the diagnosis, prevention, and prognosis of HCC. Finally, we should see that *in vitro*, 3D models based on traditional tissue engineering ideas are far from simulating real tissues and organs.[84] The 3D bioprinting technology provides a new development direction for solving this bottleneck in scientific research.[85, 86] In future research, based on the resting

bionic tumor microenvironment model, 3D bioprinting technology can be applied, or even combined with microfluidic organ chips, to build a more bionic dynamic 3D micro-environment model of HCC.

Declarations

Conflict of Interest

The authors have no conflict of interest.

Acknowledgements

This work was supported in part by the National Natural Science Foundation of China (grant no. 32101062 and no. 82072029); Guangdong Basic and Applied Basic Research Foundation (2019A1515110005); and the National high-level talents special support plan- "Ten thousand plan"-Young top-notch talent support program.

References

1. Bray, F., et al., *Global cancer statistics 2018: GLOBOCAN estimates of incidence and mortality worldwide for 36 cancers in 185 countries.* CA Cancer J Clin, 2018. **68**(6): p. 394-424.
2. Moon, H., et al., *High Risk of Hepatocellular Carcinoma Development in Fibrotic Liver: Role of the Hippo-YAP/TAZ Signaling Pathway.* Int J Mol Sci, 2019. **20**(3).
3. Novikova, M.V., N.V. Khromova, and P.B. Kopnin, *Components of the Hepatocellular Carcinoma Microenvironment and Their Role in Tumor Progression.* Biochemistry (Mosc), 2017. **82**(8): p. 861-873.
4. Campbell, J.P., et al., *Models of bone metastasis.* J Vis Exp, 2012(67): p. e4260.
5. Trautwein, C., et al., *Hepatic fibrosis: Concept to treatment.* J Hepatol, 2015. **62**(1 Suppl): p. S15-24.
6. Hoarau-Vechot, J., et al., *Halfway between 2D and Animal Models: Are 3D Cultures the Ideal Tool to Study Cancer-Microenvironment Interactions?* Int J Mol Sci, 2018. **19**(1).
7. Liu, C., et al., *Heterogeneous microenvironmental stiffness regulates pro-metastatic functions of breast cancer cells.* Acta Biomater, 2021. **131**: p. 326-340.
8. Pickl, M. and C.H. Ries, *Comparison of 3D and 2D tumor models reveals enhanced HER2 activation in 3D associated with an increased response to trastuzumab.* Oncogene, 2009. **28**(3): p. 461-8.
9. Calitz, C., et al., *A Biomimetic Model for Liver Cancer to Study Tumor-Stroma Interactions in a 3D Environment with Tunable Bio-Physical Properties.* J Vis Exp, 2020(162).
10. Prestigiacomo, V., et al., *Pro-fibrotic compounds induce stellate cell activation, ECM-remodelling and Nrf2 activation in a human 3D-multicellular model of liver fibrosis.* PLoS One, 2017. **12**(6): p. e0179995.

11. Cuvellier, M., et al., *3D culture of HepaRG cells in GelMa and its application to bioprinting of a multicellular hepatic model.* Biomaterials, 2021. **269**: p. 120611.
12. Liu, C., et al., *Hybrid collagen alginate hydrogel as a platform for 3D tumor spheroid invasion.* Acta Biomater, 2018. **75**: p. 213-225.
13. Thakuri, P.S., et al., *Biomaterials-Based Approaches to Tumor Spheroid and Organoid Modeling.* Adv Healthc Mater, 2018. **7**(6): p. e1700980.
14. Liu, C., et al., *Mammary fibroblasts remodel fibrillar collagen microstructure in a biomimetic nanocomposite hydrogel.* Acta Biomater, 2019. **83**: p. 221-232.
15. Zeisberg, M., et al., *De-differentiation of primary human hepatocytes depends on the composition of specialized liver basement membrane.* Mol Cell Biochem, 2006. **283**(1-2): p. 181-9.
16. Borlak, J., P.K. Singh, and I. Rittelmeyer, *Regulation of Liver Enriched Transcription Factors in Rat Hepatocytes Cultures on Collagen and EHS Sarcoma Matrices.* PLoS One, 2015. **10**(4): p. e0124867.
17. Ishikawa, M., et al., *Reconstitution of hepatic tissue architectures from fetal liver cells obtained from a three-dimensional culture with a rotating wall vessel bioreactor.* J Biosci Bioeng, 2011. **111**(6): p. 711-8.
18. Landry, J., et al., *Spheroidal Aggregate Culture of Rat Liver Cells: Histotypic Reorganization, Biomatrix Deposition, and Maintenance of Functional Activities.* The Journal of Cell Biology, 1985. **101**(3): p. 914-923.
19. Tran Van Nhieu, J., et al., *Myofibroblasts and hepatocellular carcinoma: an in vivo and in vitro study.* Journal of Hepatology, 1998. **29**(1): p. 120-128.
20. Zhang, H., et al., *Adenovirusmediated knockdown of activin A receptor type 2A attenuates immuneinduced hepatic fibrosis in mice and inhibits interleukin17induced activation of primary hepatic stellate cells.* Int J Mol Med, 2018. **42**(1): p. 279-289.
21. Amicone, L. and A. Marchetti, *Microenvironment and tumor cells: two targets for new molecular therapies of hepatocellular carcinoma.* Transl Gastroenterol Hepatol, 2018. **3**: p. 24.
22. Abergel, A., et al., *Growth arrest and decrease of alpha-SMA and type I collagen expression by palmitic acid in the rat hepatic stellate cell line PAV-1.* Dig Dis Sci, 2006. **51**(5): p. 986-95.
23. Sancho-Bru, P., et al., *Hepatocarcinoma cells stimulate the growth, migration and expression of pro-angiogenic genes in human hepatic stellate cells.* Liver Int, 2010. **30**(1): p. 31-41.
24. Fu, B.H., Z.Z. Wu, and J. Qin, *Effects of integrins on laminin chemotaxis by hepatocellular carcinoma cells.* Mol Biol Rep, 2010. **37**(3): p. 1665-70.
25. Caja, L., et al., *The transforming growth factor-beta (TGF-beta) mediates acquisition of a mesenchymal stem cell-like phenotype in human liver cells.* J Cell Physiol, 2011. **226**(5): p. 1214-23.
26. Crystal, R.G., *Alpha 1-antitrypsin deficiency, emphysema, and liver disease. Genetic basis and strategies for therapy.* J Clin Invest, 1990. **85**(5): p. 1343-52.
27. Toro, H., et al., *Serum chemistry and antibody status to some avian pathogens of free-living and captive condors (Vultur gryphus) of central Chile.* Avian Pathol, 1997. **26**(2): p. 339-45.

28. Huang, Q., et al., *The relationship between liver-kidney impairment and viral load after nephropathogenic infectious bronchitis virus infection in embryonic chickens.* Poult Sci, 2017. **96**(6): p. 1589-1597.
29. Ma, S., et al., *Identification and characterization of tumorigenic liver cancer stem/progenitor cells.* Gastroenterology, 2007. **132**(7): p. 2542-56.
30. Jiang, Y., et al., *Upregulation of Serum Sphingosine (d18:1)-1-P Potentially Contributes to Distinguish HCC Including AFP-Negative HCC From Cirrhosis.* Front Oncol, 2020. **10**: p. 1759.
31. Li, W., et al., *The Clinical Significance of PIWIL3 and PIWIL4 Expression in Pancreatic Cancer.* J Clin Med, 2020. **9**(5).
32. Stoffel, M. and S.A. Duncan, *The maturity-onset diabetes of the young (MODY1) transcription factor HNF4alpha regulates expression of genes required for glucose transport and metabolism.* Proc Natl Acad Sci U S A, 1997. **94**(24): p. 13209-14.
33. Hamdan, F.H. and M.A. Zihlif, *Gene expression alterations in chronic hypoxic MCF7 breast cancer cell line.* Genomics, 2014. **104**(6 Pt B): p. 477-81.
34. Betts, S., et al., *Expression of CYP3A4 and CYP3A7 in Human Foetal Tissues and its Correlation with Nuclear Receptors.* Basic Clin Pharmacol Toxicol, 2015. **117**(4): p. 261-6.
35. Hines, R.N., *Ontogeny of human hepatic cytochromes P450.* 2007. **21**(4): p. 169-175.
36. Lacroix, D., et al., *Expression of CYP3A in the Human Liver — Evidence that the Shift between CYP3A7 and CYP3A4 Occurs Immediately After Birth.* European Journal of Biochemistry, 1997. **247**(2): p. 625-634.
37. Wilkening, S. and A. Bader, *Differential regulation of CYP3A4 and CYP3A7 by dimethylsulfoxide in primary human hepatocytes.* Basic Clin Pharmacol Toxicol, 2004. **95**(2): p. 92-3.
38. Katagiri, A., et al., *MEK inhibition suppresses cell invasion and migration in ovarian cancers with activation of ERK1/2.* Exp Ther Med, 2010. **1**(4): p. 591-596.
39. Bi, W.R., et al., *Bone morphogenetic protein-7 regulates Snail signaling in carbon tetrachloride-induced fibrosis in the rat liver.* Exp Ther Med, 2012. **4**(6): p. 1022-1026.
40. Kang, Y. and J. Massague, *Epithelial-mesenchymal transitions: twist in development and metastasis.* Cell, 2004. **118**(3): p. 277-9.
41. Gravdal, K., et al., *A switch from E-cadherin to N-cadherin expression indicates epithelial to mesenchymal transition and is of strong and independent importance for the progress of prostate cancer.* Clin Cancer Res, 2007. **13**(23): p. 7003-11.
42. Tran, N.L., et al., *N-Cadherin Expression in Human Prostate Carcinoma Cell Lines.* The American Journal of Pathology, 1999. **155**(3): p. 787-798.
43. Christiansen, J.J. and A.K. Rajasekaran, *Reassessing epithelial to mesenchymal transition as a prerequisite for carcinoma invasion and metastasis.* Cancer Res, 2006. **66**(17): p. 8319-26.
44. Thiery, J.P., *Epithelial-mesenchymal transitions in tumour progression.* Nat Rev Cancer, 2002. **2**(6): p. 442-54.

45. Hazan, R.B., et al., *Cadherin switch in tumor progression.* Ann N Y Acad Sci, 2004. **1014**: p. 155-63.
46. Maria, J.C. and D.R. David, *Novel Integrin Antagonists Derived from Thrombospondins.* Current Pharmaceutical Design, 2005. **11**(7): p. 849-866.
47. Reglero-Real, N., B. Marcos-Ramiro, and J. Millan, *Endothelial membrane reorganization during leukocyte extravasation.* Cell Mol Life Sci, 2012. **69**(18): p. 3079-99.
48. Li, M., et al., *Na(+) /H(+) exchanger regulatory factor 1 knockout mice have an attenuated hepatic inflammatory response and are protected from cholestatic liver injury.* Hepatology, 2015. **62**(4): p. 1227-36.
49. Jin, H., et al., *ESM-1 Overexpression is Involved in Increased Tumorigenesis of Radiotherapy-Resistant Breast Cancer Cells.* Cancers (Basel), 2020. **12**(6).
50. Gaça, M.D.A., et al., *Basement membrane-like matrix inhibits proliferation and collagen synthesis by activated rat hepatic stellate cells: evidence for matrix-dependent deactivation of stellate cells.* Matrix Biology, 2003. **22**(3): p. 229-239.
51. Schnabl, B., et al., *Immortal Activated Human Hepatic Stellate Cells Generated by Ectopic Telomerase Expression.* Laboratory Investigation, 2002. **82**(3): p. 323-333.
52. Natarajan, V., et al., *Substrate stiffness regulates primary hepatocyte functions.* RSC Advances, 2015. **5**(99): p. 80956-80966.
53. Desai, S.S., et al., *Physiological ranges of matrix rigidity modulate primary mouse hepatocyte function in part through hepatocyte nuclear factor 4 alpha.* Hepatology, 2016. **64**(1): p. 261-75.
54. Li, C.Y., et al., *Micropatterned cell-cell interactions enable functional encapsulation of primary hepatocytes in hydrogel microtissues.* Tissue Eng Part A, 2014. **20**(15-16): p. 2200-12.
55. Anttila, M.A., et al., *High levels of stromal hyaluronan predict poor disease outcome in epithelial ovarian cancer.* Cancer Res, 2000. **60**(1): p. 150-5.
56. Liu, N., et al., *Metastatin: a hyaluronan-binding complex from cartilage that inhibits tumor growth.* Cancer Res, 2001. **61**(3): p. 1022-8.
57. Xu, X., et al., *Hyaluronic Acid-Based Hydrogels: from a Natural Polysaccharide to Complex Networks.* Soft Matter, 2012. **8**(12): p. 3280-3294.
58. Liu, C., et al., *Heterogeneous microenvironmental stiffness regulates pro-metastatic functions of breast cancer cells.* Acta Biomater, 2021: p. 7471.
59. Fennema, E., et al., *Spheroid culture as a tool for creating 3D complex tissues.* Trends Biotechnol, 2013. **31**(2): p. 108-15.
60. Kobayashi, A., et al., *Regulation of Differentiation and Proliferation of Rat Hepatocytes by Lactose-Carrying Polystyrene.* Artificial Organs, 1992. **16**(6): p. 564-567.
61. Tostoes, R.M., et al., *Human liver cell spheroids in extended perfusion bioreactor culture for repeated-dose drug testing.* Hepatology, 2012. **55**(4): p. 1227-36.
62. Zeigerer, A., et al., *Functional properties of hepatocytes in vitro are correlated with cell polarity maintenance.* Exp Cell Res, 2017. **350**(1): p. 242-252.

63. Moghe, P.V., et al., *Culture matrix configuration and composition in the maintenance of hepatocyte polarity and function.* Biomaterials, 1996. **17**(3): p. 373-385.
64. Ballatori, N., et al., *Retention of structural and functional polarity in cultured skate hepatocytes undergoing in vitro morphogenesis.* Comp Biochem Physiol B Biochem Mol Biol, 2006. **144**(2): p. 167-79.
65. Khetani, S.R. and S.N. Bhatia, *Microscale culture of human liver cells for drug development.* Nat Biotechnol, 2008. **26**(1): p. 120-6.
66. Sun, P., et al., *Maintenance of Primary Hepatocyte Functions In Vitro by Inhibiting Mechanical Tension-Induced YAP Activation.* Cell Rep, 2019. **29**(10): p. 3212-3222 e4.
67. Xiang, C., et al., *Long-term functional maintenance of primary human hepatocytes in vitro.* Science, 2019. **364**(6438): p. 399-402.
68. Grover, A., R.G. Oshima, and E.D. Adamson, *Epithelial layer formation in differentiating aggregates of F9 embryonal carcinoma cells.* J Cell Biol, 1983. **96**(6): p. 1690-6.
69. Grover, A., G. Andrews, and E.D. Adamson, *Role of laminin in epithelium formation by F9 aggregates.* Journal of Cell Biology, 1983. **97**(1): p. 137-144.
70. Serna-Marquez, N., et al., *Fibrillar Collagen Type I Participates in the Survival and Aggregation of Primary Hepatocytes Cultured on Soft Hydrogels.* Biomimetics (Basel), 2020. **5**(2).
71. Coulouarn, C. and B. Clement, *Stellate cells and the development of liver cancer: therapeutic potential of targeting the stroma.* J Hepatol, 2014. **60**(6): p. 1306-9.
72. Friedman, S.L., *Mechanisms of hepatic fibrogenesis.* Gastroenterology, 2008. **134**(6): p. 1655-69.
73. Ju, M.J., et al., *Peritumoral activated hepatic stellate cells predict poor clinical outcome in hepatocellular carcinoma after curative resection.* Am J Clin Pathol, 2009. **131**(4): p. 498-510.
74. Omer, R.E., et al., *Population-attributable risk of dietary aflatoxins and hepatitis B virus infection with respect to hepatocellular carcinoma.* Nutr Cancer, 2004. **48**(1): p. 15-21.
75. van Zijl, F., et al., *Hepatic tumor-stroma crosstalk guides epithelial to mesenchymal transition at the tumor edge.* Oncogene, 2009. **28**(45): p. 4022-33.
76. Wang, Y., et al., *ECM proteins in a microporous scaffold influence hepatocyte morphology, function, and gene expression.* Sci Rep, 2016. **6**: p. 37427.
77. Yang, Y., et al., *Downregulated connexin32 promotes EMT through the Wnt/beta-catenin pathway by targeting Snail expression in hepatocellular carcinoma.* Int J Oncol, 2017. **50**(6): p. 1977-1988.
78. Capece, D., et al., *The inflammatory microenvironment in hepatocellular carcinoma: a pivotal role for tumor-associated macrophages.* Biomed Res Int, 2013. **2013**: p. 187204.
79. Zhai, X., et al., *The beta-catenin pathway contributes to the effects of leptin on SREBP-1c expression in rat hepatic stellate cells and liver fibrosis.* Br J Pharmacol, 2013. **169**(1): p. 197-212.
80. Nieto, M.A. and A. Cano, *The epithelial-mesenchymal transition under control: global programs to regulate epithelial plasticity.* Semin Cancer Biol, 2012. **22**(5-6): p. 361-8.

81. Garrido, A. and N. Djouder, *Cirrhosis: A Questioned Risk Factor for Hepatocellular Carcinoma.* Trends Cancer, 2021. **7**(1): p. 29-36.
82. Charras, G. and E. Sahai, *Physical influences of the extracellular environment on cell migration.* Nat Rev Mol Cell Biol, 2014. **15**(12): p. 813-24.
83. Yang, H.W., et al., *An investigation of the distribution and location of mast cells affected by the stiffness of substrates as a mechanical niche.* Int J Biol Sci, 2018. **14**(9): p. 1142-1152.
84. Moreau, J.E., et al., *Tissue-engineered bone serves as a target for metastasis of human breast cancer in a mouse model.* Cancer Res, 2007. **67**(21): p. 10304-8.
85. Alemany-Ribes, M. and C.E. Semino, *Bioengineering 3D environments for cancer models.* Adv Drug Deliv Rev, 2014. **79-80**: p. 40-9.
86. Kwakwa, K.A., et al., *Engineering 3D Models of Tumors and Bone to Understand Tumor-Induced Bone Disease and Improve Treatments.* Curr Osteoporos Rep, 2017. **15**(4): p. 247-254.

Figures

Figure 1

Construction and observations of 3D bionic HCC microenvironment model. a, the flow chart of HCC microenvironment model construction. Scale bar indicates 200 μm. b, imaging of hepatoma cells (blue), normal hepatocytes (green), and hepatic stellate cell spheroids (red) in the HCC microenvironment model. Scale bar indicates 200 μm. c and d, the 3D plot and histogram of the results of nanoindentation tests. Scale bar indicates 58.04–312.89 Pa. e, imaging of the lumen-like microstructure by inverted fluorescence microscope on day 0, 1, 2, 5, and 7. The hepatic canaliculi and canaliculi-like structures were annotated with white arrows. Scale bar indicates 200 μm.

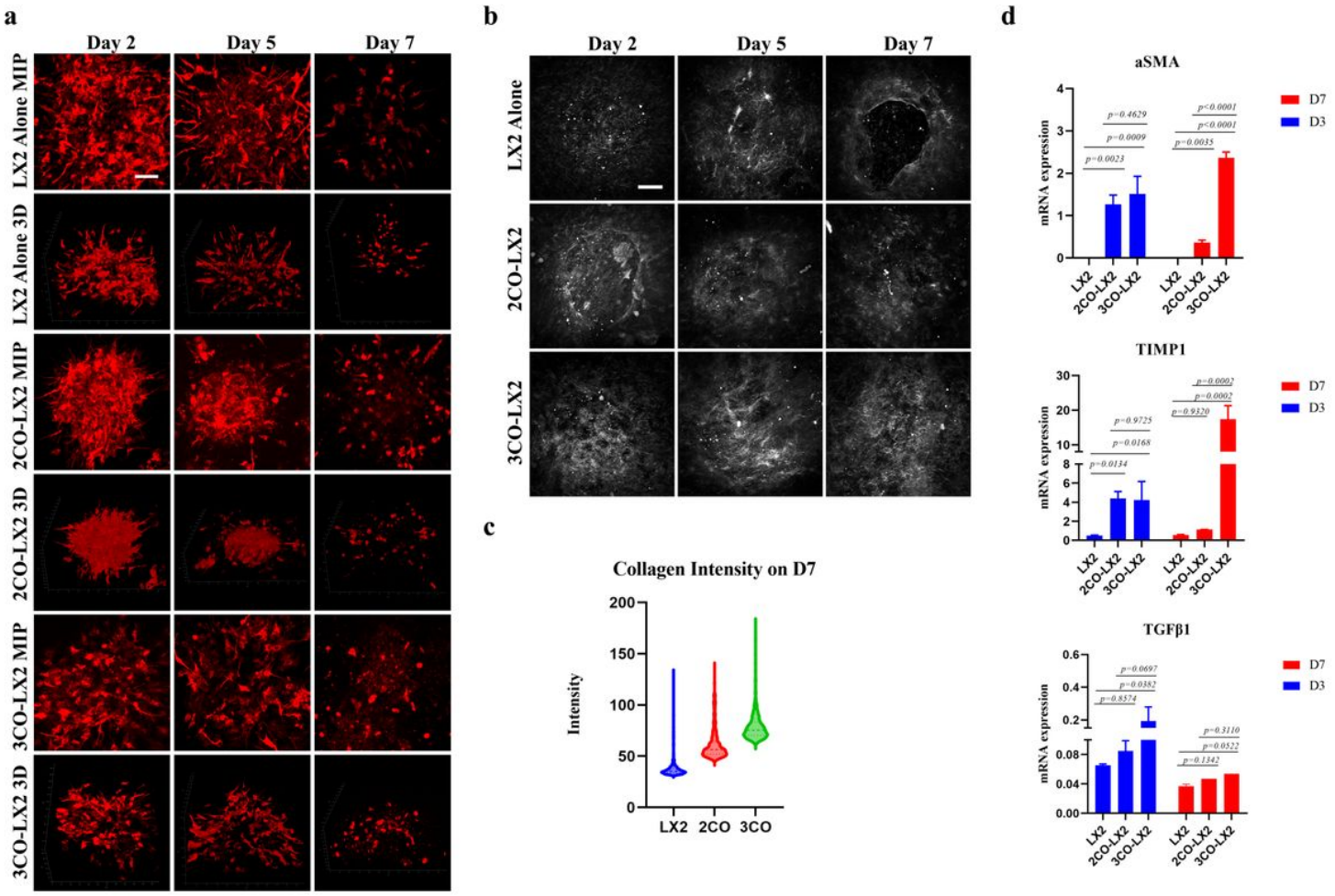

Figure 2

Activated hepatic stellate cell induced by hepatoma cells promotes hepatic fibrosis. a, imaging of morphological changes of LX2 hepatic stellate cells in each culture system on day 2, 5, and 7. 2CO: HL-7702 cell spheroids with LX2 cell spheroids. 3CO: HL-7702 cell spheroids, LX2 cell spheroids and MHCC-97H cell spheroids. MIP: maximum intensity projection. Scale bar indicates 100 μm. b, two-photon imaging of collagen deposition in each culture system on day 2, 5, and 7. Scale bar indicates 100μm. c, the violin chart of the fluorescence intensity of collagen in two-photon imaging. d, total RNA was extracted from hydrogels recovered from human. The expression levels of α-SMA, TIMP1 and TGF-β1 genes related to HSCs activation were detected by RT-qPCR on day 3 and 7. Error bars represent standard deviations of three independent experiments. p values were shown as indicated in graph. Significance was indicated as $p < 0.05$.

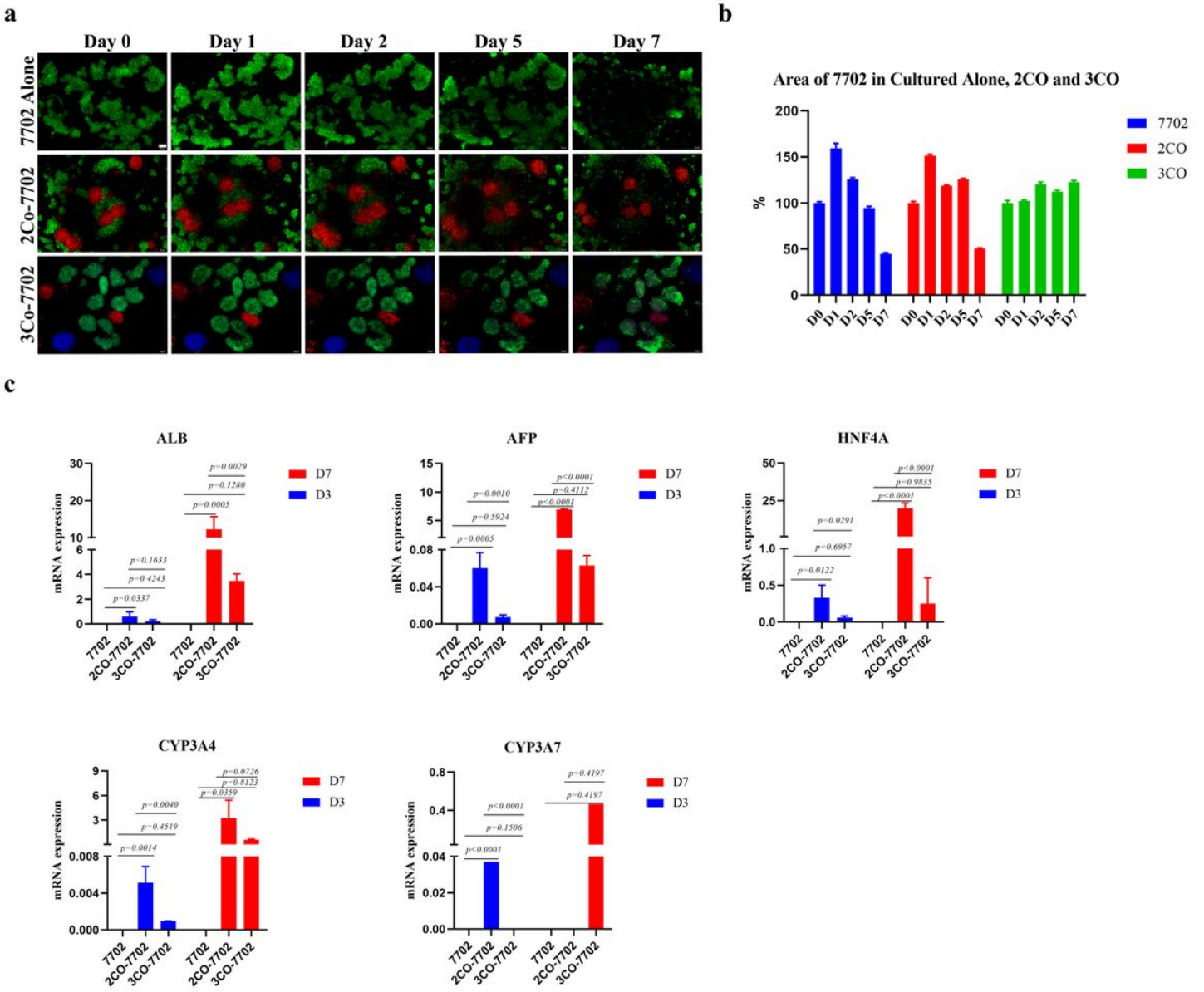

Figure 3

Effect of activation of hepatic stellate cells on normal hepatocytes. a, HL-7702 hepatocytes were imaged by ordinary fluorescence microscope on day 0, 1, 2, 5, and 7. 2CO: HL-7702 cell spheroids with LX2 cell spheroids. 3CO: HL-7702 cell spheroids, LX2 cell spheroids and MHCC-97H cell spheroids. Scale bar indicates 200 μm. b, the chart bar of the area of 7702 in the different cultured systems. c, quantitative detection of ALB, AFP, HNF4A, CYP3A4, and CYP3A7 gene expression in normal hepatocytes by RT-qPCR on the day 3 and 7. Error bars represent standard deviations of three independent experiments. p values were shown as indicated in the graph. Significance was indicated as $p < 0.05$.

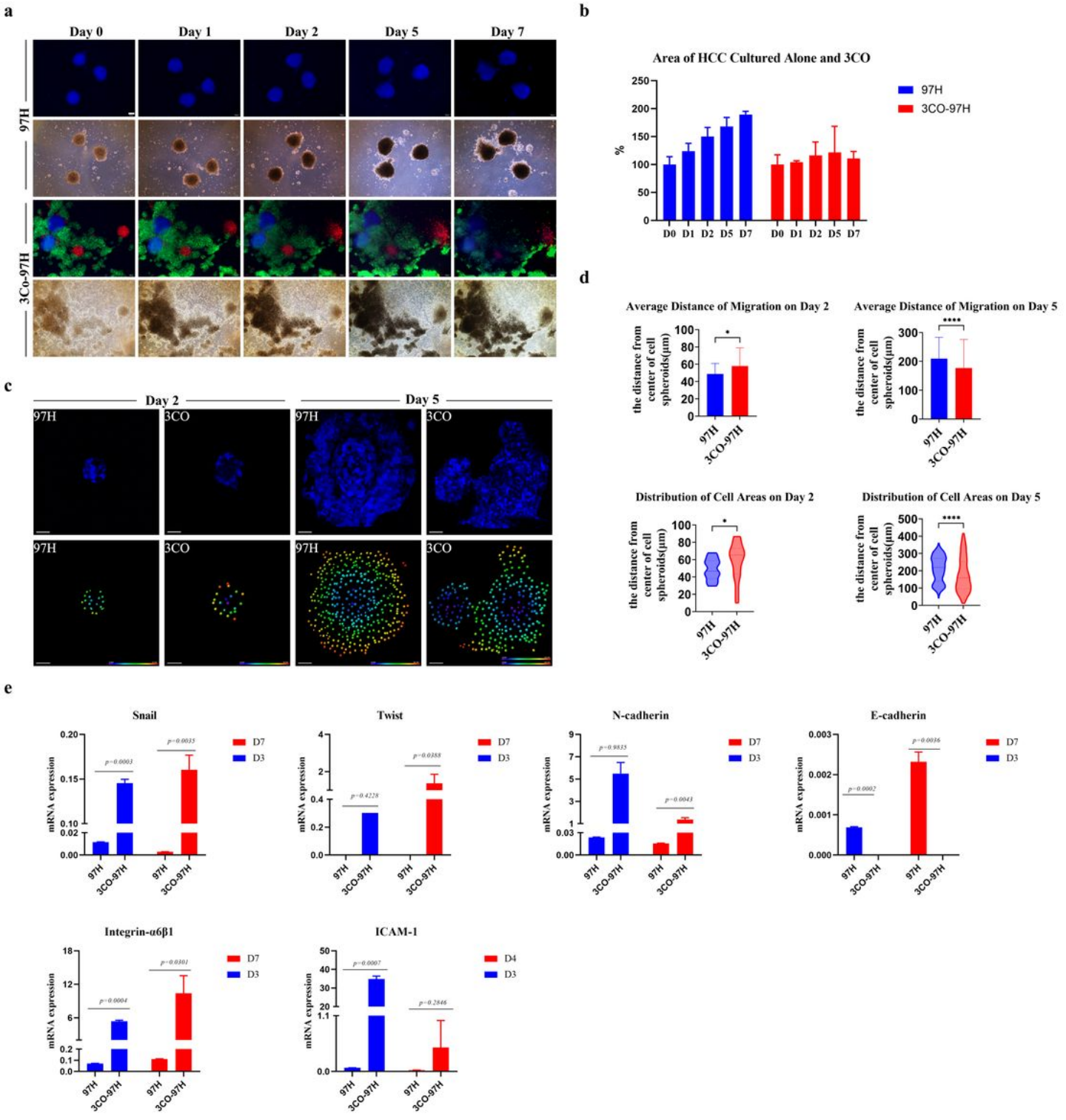

Figure 4

The proliferation and migration of cancer cells in the HCC microenvironment model. a, MHCC-97H hepatoma cell spheroids were imaged by ordinary fluorescence microscope on day 0,1,2,5, and 7. 3CO: HL-7702 cell spheroids, LX2 cell spheroids and MHCC-97H cell spheroids. Scale bar indicates 200 μm. b, the chart bar of the area of HCC cultured alone and 3CO. c, two-photon microscope imaging of MHCC-97H hepatoma cell spheroids in the single culture system and in HCC microenvironment model. Scale bar

indicates 100 μm. d, the bar charts and violin charts of the average distance and distribution of calculation. ∗: p < 0.05; ****: p < 0.0001. e, the gene expression levels of Snail, Twist, N-cadherin, E-cadherin, Integrin α6β1, and ICAM-1 in HCC cells were detected on day 3 and 7 by RT-qPCR. Error bars represent standard deviations of three independent experiments. p values were shown as indicated in the graph. Significance was indicated as p < 0.05.

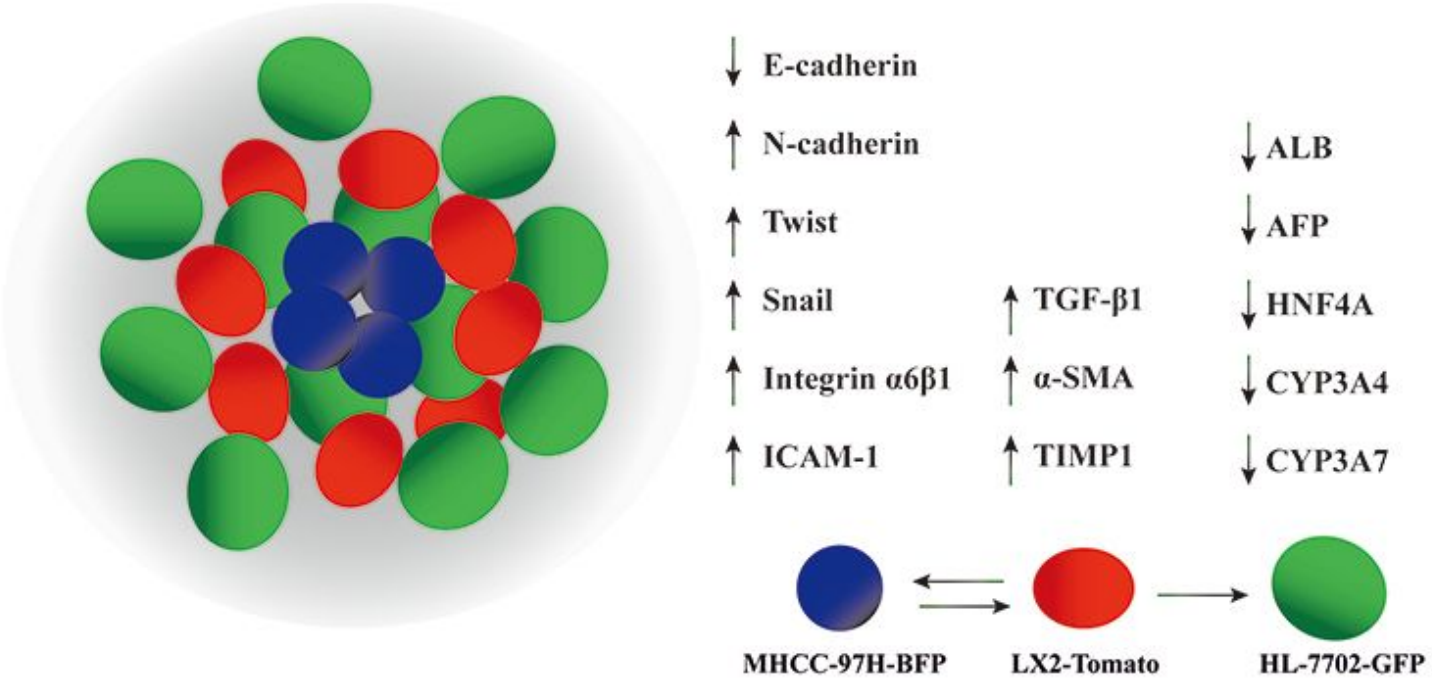

Figure 5

Schematic diagram of co-culture of HCCs, HSCs, and normal hepatocytes spheroids and the rise and fall of related gene expression.